

This discussion paper is/has been under review for the journal *Climate of the Past* (CP).  
Please refer to the corresponding final paper in CP if available.

# Scaling laws for perturbations in the ocean–atmosphere system following large CO<sub>2</sub> emissions

N. Towles, P. Olson, and A. Gnanadesikan

Department of Earth and Planetary Sciences, Johns Hopkins University, Baltimore, MD 21218, USA

Received: 4 November 2014 – Accepted: 24 November 2014 – Published: 23 January 2015

Correspondence to: N. Towles (nathan.towles@gmail.com)

Published by Copernicus Publications on behalf of the European Geosciences Union.

95

## Abstract

Scaling relationships are derived for the perturbations to atmosphere and ocean variables from large transient CO<sub>2</sub> emissions. Using the carbon cycle model LOSCAR (Zeebe et al., 2009; Zeebe, 2012b) we calculate perturbations to atmosphere temperature and total carbon, ocean temperature, total ocean carbon, pH, and alkalinity, marine sediment carbon, plus carbon-13 isotope anomalies in the ocean and atmosphere resulting from idealized CO<sub>2</sub> emission events. The peak perturbations in the atmosphere and ocean variables are then fit to power law functions of the form  $\gamma D^\alpha E^\beta$ , where  $D$  is the event duration,  $E$  is its total carbon emission, and  $\gamma$  is a coefficient. Good power law fits are obtained for most system variables for  $E$  up to 50 000 PgC and  $D$  up to 100 kyr. However, these power laws deviate substantially from predictions based on simplified equilibrium considerations. For example, although all of the peak perturbations increase with emission rate  $E/D$ , we find no evidence of emission rate-only scaling  $\alpha + \beta = 0$ , a prediction of the long-term equilibrium between CO<sub>2</sub> input by volcanism and CO<sub>2</sub> removal by silicate weathering. Instead, our scaling yields  $\alpha + \beta \simeq 1$  for total ocean and atmosphere carbon and  $0 < \alpha + \beta < 1$  for most of the other system variables. The deviations in these scaling laws from equilibrium predictions are mainly due to the multitude and diversity of time scales that govern the exchange of carbon between marine sediments, the ocean, and the atmosphere.

## 1 Introduction

The study of how the Earth system responds to large, transient carbon emissions is of particular importance for developing a better understanding of our past, present, and future climate. Eruptions of super volcanoes, extrusion of flood basalts, dissociation of methane hydrates, and widespread anthropogenic burning of fossil fuels are a few examples of these types of emissions.

96

What complicates our understanding of the response to these transient perturbations is the fact that there are many carbon reservoirs with a large range of intrinsic timescales associated with the different processes governing the Earth system. On timescales  $< 10^3$  years, exchanges between the atmosphere, biosphere, soils and ocean occur. On time scales  $10^3 - 10^5$  years, ocean carbonate-sediment interactions become significant (Archer et al., 2009). When dealing with timescales  $> 10^5$  years it becomes necessary to consider effects of geologic processes such as silicate weathering, as these control how the system resets to an equilibrium balance. The complex interactions between so many system components over such a large range of timescales make it difficult to predict how the Earth responds to  $\text{CO}_2$  perturbations of different magnitudes and durations.

In general, the modeling of carbon perturbations is undertaken for two purposes. One is to predict future system changes that are expected to occur as a result of a particular emission history, such as the history of anthropogenic emissions in the industrial age. The other purpose is to infer the sizes and durations of carbon perturbations in the past, by comparing model results with various recorders of environmental change. According to an often-used model based on simplified considerations of atmospheric equilibrium, the long-term abundance of  $\text{CO}_2$  in the Earth system is determined by a balance between the injection of carbon into the atmosphere in the forms of volcanic and metamorphic emissions and the removal of atmospheric carbon through weathering of silicates and subsequent burial of marine carbonate sediments (Walker et al., 1981; Berner and Kothavala, 2001; Berner and Caldeira, 1997; Zeebe, 2012b; Uchikawa and Zeebe, 2008). This balance predicts that the very slow changes in atmospheric carbon should scale with the rate of emissions, and in addition, should exhibit a strong sensitivity to the functional form of silicate weathering, that is, its dependence on temperature and atmospheric  $\text{CO}_2$  content (Walker et al., 1981). This particular balance has been widely used in paleoclimate studies because it offers a concise interpretation of past climate events in terms of changes in the rate of carbon

emission. However, relatively little attention has been paid to questions of how well this balance applies to transient emissions with widely varying magnitudes and durations.

We are interested in the response of the Earth system to emission events with sizes ranging from hundreds to tens of thousands petagrams of carbon (PgC) and durations ranging from one hundred years to one hundred thousand years. In principle this information could be generated using three-dimensional Earth System Models, as it has been for anthropogenic perturbations (Sarmiento et al., 1998; Matsumoto et al., 2004). However because of their focus on short-term climate change, relatively few comprehensive Earth system models have included interactions with the sediments (an exception being the Bergen Climate Center of Tjiputra et al., 2010). Moreover, the very long run times (on the order of hundreds of thousands of years) that are necessary to capture the entire history of a perturbation represent a significant computational burden for these models, making it difficult to run enough cases to generate scaling laws. Accordingly, in this study we adopt a more streamlined approach, using a simplified Earth system model suitable for representing the carbon cycle on hundred thousand year timescales and focusing our attention on perturbations to globally-averaged properties rather than local effects.

In this paper we derive scaling laws that link perturbations of Earth system variables to atmospheric  $\text{CO}_2$  emission size and duration. We use the LOSCAR carbon cycling model (Zeebe et al., 2009; Zeebe, 2012b) to determine quantitative relationships between the magnitude of perturbations to Earth system variables such as atmospheric  $\text{CO}_2$ , ocean acidity and alkalinity, and carbon isotope anomalies and idealized transient  $\text{CO}_2$  emissions that differ only in terms of their duration and total size. Analyzing the system response to such  $\text{CO}_2$  emissions ranging in total size from 100 to 50 000 PgC and durations from 100 years to 100 kyr, we find that most Earth system variable perturbations can be scaled using power law formulas, but with exponents that differ substantially from what is expected on the basis of simplified equilibrium considerations.

## 2 Previous work

LOSCAR has been employed to investigate a range of problems for both paleo and modern climate applications. It has specifically been used to study the impacts of large transient emissions such as those found during the Paleocene-Eocene Thermal Maximum (PETM), as well as modern Anthropogenic emissions.

For paleoclimate applications LOSCAR has been used to constrain the transient emission needed to produce the observed Earth system responses found during the PETM (Zeebe et al., 2009), and more generally, to investigate the response of atmospheric CO<sub>2</sub> and ocean chemistry to carbon perturbations throughout the Cenozoic with different seawater chemistry and bathymetry (Stuecker and Zeebe, 2010). Particular applications include constraining the range of the pH effects on carbon and oxygen isotopes in organisms during the PETM perturbation (Uchikawa and Zeebe, 2010), to investigate the effects of weathering on the [Ca<sup>2+</sup>] inventory of the oceans during the PETM (Komar and Zeebe, 2011), to infer changes in ocean carbonate chemistry using the Holocene atmospheric CO<sub>2</sub> record (Zeebe, 2012a), and to investigate different processes that potentially generated large scale fluctuations in the calcite compensation depth (CCD) in the middle to late Eocene (Pälike et al., 2012). Other applications include analysis of perturbations to the carbon cycle during the Middle Eocene Climatic Optimum (MECO) (Sluijs et al., 2013), and study of effects of slow methane release during the early Paleogene (62–48 Ma) (Komar et al., 2013).

For the modern climate applications LOSCAR has been used to show how decrease in ocean pH is sensitive to carbon release time, specifically for possible future anthropogenic release scenarios (Zeebe et al., 2008), to determine whether enhanced weathering feedback can mitigate future pCO<sub>2</sub> rise (Uchikawa and Zeebe, 2008), to study effects of increasing ocean alkalinity as a means to mitigate ocean acidification and moderate atmospheric pCO<sub>2</sub> (Paquay and Zeebe, 2013), and to compare modern perturbations with those inferred during the PETM, to assess the long-term legacy of massive carbon inputs (Zeebe and Zachos, 2013).

99

## 3 Methods

Figure 1 is a schematic illustrating the type of forcing considered in this study and the nature of the Earth system response. Figure 1a shows a CO<sub>2</sub> emission event with a symmetric, triangular-shaped emission rate history superimposed on a steady background emission rate,  $R_o$ . The transient emission starts at time  $t_o$  and ends at time  $t_o + D$ , so that  $D$  is its duration. The total emission in the event,  $E$ , is related to its duration and peak emission rate,  $R_{peak}$ , by  $E = D\Delta R/2$ , where  $\Delta R = R_{peak} - R_o$ . By virtue of the assumption of symmetry,  $R_{peak}$  occurs at time  $t_o + D/2$ . Figure 1b shows the response of a typical system variable,  $V$ . The system variable changes with time from its initial value  $V_o$ , to its peak value  $V_{peak}$ , then relaxes back toward  $V_o$ . We define the peak system response as  $\Delta V = |V_{peak} - V_o|$ , the absolute value being necessary in this definition because some system variables respond with negative perturbations. In this study we seek mathematical relationships connecting  $\Delta V$  to  $D$  and  $E$ .

LOSCAR is a box model designed for these objectives. As noted above, it has been applied to a number of events in the paleoclimate record. LOSCAR components include the atmosphere and a three-layer representation of the major ocean basins (Atlantic, Indian, and Pacific) coupled to a marine sediment component (Zeebe, 2012b). The marine sediment component consists of sediment boxes in each of the major ocean basins arranged as functions of depth. The ocean component includes a representation of the mean overturning circulation as well as mixing. Biological cycling is parameterized by surface nutrients to fixed values. In the simulations described here, the circulation and target surface nutrients are kept independent of climate change, so that we focus solely on contrasting surface weathering and sedimentary responses. Biogeochemical cycling in LOSCAR also includes calcium carbonate (CaCO<sub>3</sub>) dissolution, weathering and burial, silicate weathering and burial, calcite compensation, plus carbon fluxes between the sediments, the ocean basins, and the atmosphere. Carbonate dissolution is limited by including variable sediment porosity. In addition, LOSCAR includes a high-latitude surface ocean box without

sediments but otherwise coupled to the other ocean basins through circulation and mixing. Table 3 lists the important model variables, including their notation and dimensional units.

#### 4 Case study results

5 Figures 2–7 show the LOSCAR response to an emission event with size  $E = 1000$  PgC and duration  $D = 5$  kyr of the type illustrated in Fig. 1. This particular example was initialized using steady-state preindustrial conditions with an atmospheric  $p\text{CO}_2 = 280$  ppmv corresponding to a total atmosphere carbon content,  $\text{TC}_{\text{atm}} = 616$  PgC. The initial total carbon content of the global oceans was  $\text{TC}_{\text{ocn}} = 35\,852$  PgC and the initial  
10 global ocean total alkalinity (TA) was  $\text{TA} = 3.1377 \times 10^{18}$  mol. The emission event began 100 years after startup and its duration is indicated by shading in the figures. This calculation, like all of the others in this study, spans 5 Myr in order to ensure that final equilibrium conditions are reached.

The resulting changes in total ocean and atmosphere carbon,  $\text{TC}_{\text{ocn}}$  and  $\text{TC}_{\text{atm}}$  respectively, are shown in Fig. 2a as functions of time in log units. The atmosphere peak perturbation occurs 3744 years after emission onset, whereas the ocean perturbation peaks 26440 years after emission onset. The inflection point in the atmosphere response nearly corresponds to the peak ocean response and is an example of the *carbon tail* phenomenon. This particular carbon tail is due to ocean-sediment  
20 interactions and differs from the carbon tail described by Archer et al. (2009), which is controlled primarily by silicate weathering fluxes.

Figure 2b shows the corresponding rates of change of  $\text{TC}_{\text{ocn}}$  and  $\text{TC}_{\text{atm}}$ . The curves labeled Atm and Ocn are the time derivatives from Fig. 2a, and the curve labeled Total is their sum. Also shown in Fig. 2b is the adjusted total, the difference  
25 between the total rate of change in the atmosphere + ocean and  $R - R_0$ . The adjusted total, which corresponds to the rate at which additional carbon is added to the ocean–atmosphere system through the reactive processes of weathering,  $\text{CaCO}_3$

101

dissolution, and calcite compensation, peaks at  $0.16$  PgCyr $^{-1}$  and is positive for about the first 10 kyr after emission onset. This behavior demonstrates how these reactive processes amplify the carbon perturbation coming directly from an emission event. The logarithmic time scale (necessary to capture both the fast rise and slow fall-off of  
5 the carbon perturbation) obscures the important fact that these reactive processes play a quantitatively significant role, accounting for a significant fraction of the large rise in oceanic carbon that occurs after the atmospheric peak.

Because additional carbon enters the system through reactive processes of weathering and marine sediment dissolution and leaves the system through deposition,  
10 the total carbon perturbation at any given time generally does not equal the total emission up to that time. To quantify this effect we define gain factors, which are ratios of total carbon perturbation to total emission measured at time  $t$ . For the atmosphere and ocean these are:

$$G_{\text{atm}}(t) = \frac{\text{TC}_{\text{atm}}(t) - \text{TC}_{\text{atm}}(t_0)}{E(t)} \quad (1)$$

$$15 \quad G_{\text{ocn}}(t) = \frac{\text{TC}_{\text{ocn}}(t) - \text{TC}_{\text{ocn}}(t_0)}{E(t)}. \quad (2)$$

We also define gain factors for the ocean–atmosphere system as

$$G_{\text{sys}}^+(t) = G_{\text{atm}}(t) + G_{\text{ocn}}(t) \quad (3)$$

$$G_{\text{sys}}^-(t) = G_{\text{atm}}(t) - G_{\text{ocn}}(t). \quad (4)$$

According to these definitions,  $G_{\text{sys}}^+$  is the gain of the system as a whole.  $G_{\text{sys}}^-$  gives  
20 information on the time dependent partitioning of carbon between the atmosphere and ocean reservoirs.

Figure 3 shows these gain factors as a function of time for the emission event from Fig. 2.  $G_{\text{atm}}$  decreases monotonically over the duration of the emission; the small residual in  $G_{\text{atm}}$  following the emission is an example of the classical carbon tail (Archer

102

et al., 2009). In contrast,  $G_{\text{ocn}}$  rises during the emission and continues to increase until it peaks at 1.68, 26 438 years after emission onset, then decreases to unity after 378 850 years, and finally returns to zero. Similarly,  $G_{\text{sys}}^+$  generally rises during the emission, peaking at a value of 1.76 around 25 000 years after emission onset, then decreasing to unity after 408 260 years.  $G_{\text{sys}}^-$  is almost a mirror image of  $G_{\text{ocn}}$ , indicating that the sediments are contributing more carbon to the ocean than to the atmosphere during this time.

The response of the ocean layers is shown in Fig. 4. Figure 4a shows the time variations in pH in each ocean layer as well as the global ocean total alkalinity. Note that pH variations lead TA in time; first pH drops and TA begins to rise in response, then pH recovers and later TA recovers. The minima in the ocean surface, intermediate, and deep layer pH occur 3618, 3797, and 4600 years respectively, after emission onset. In contrast, the maximum TA occurs 30 455 years after emission onset (by which time the the pH is almost fully recovered) and the TA does not fully recover for more than one million years.

Effects of the emission event on Atlantic Ocean sediments are shown in Fig. 4b. The deeper sediments respond earlier and take longer to recover from the perturbation compared to the shallower sediments. In addition, the sediments at 5000 and 5500m depths do not recover monotonically, but instead overshoot their initial state, becoming relatively enriched in carbonate for tens of thousands of years. This transient enrichment process has been explained by Zeebe (2012b) as a direct consequence of the weathering feedback, where the enhanced weathering, due to elevated  $p\text{CO}_2$ , increases the ocean saturation state and deepens the CCD to balance the riverine and burial fluxes.

Figure 4c shows the unweighted average temperature perturbations, which contrast with TA by recovering on timescales of order thousands of years, rather than tens of thousands. Peak temperatures perturbations occur between 3743 and 4814 years after emission onset. Although the atmospheric temperature mostly recovers after a couple of thousands of years, there remains a small anomaly for longer periods due to coupling

103

with  $p\text{CO}_2$  in the atmosphere, which as discussed before has an extended carbon tail for up to millions of years, depending on the strength of prescribed weathering feedbacks (Archer et al., 2009; Komar and Zeebe, 2011).

Figure 5 shows the sediment carbonate content for each ocean basin as a function of depth, with colors indicating the starting, maximum, and minimum values that were recorded in each depth box. The deep boxes are most perturbed because they are directly affected by movement of the CCD. In addition, sediments in the deep Atlantic are perturbed more than those in the Pacific or Indian basins because the CCD is deeper in the Atlantic. Far more carbon enrichment occurs in the Atlantic, for example, the 5000 m box starts at 22 % carbonate and during the run increases to close to 50 %. Figure 6 shows the time derivative of global TA for the aforementioned case. The red curve accounts for the known contributions of TA from weathering feedbacks and therefore depicts the alkalinity flux that is due to dissolution, and subsequent burial of marine carbonates. Where the red curve is positive it denotes a net dissolution of carbonates; where it is negative it denotes a net burial of carbonates. The peak fluxes occur 3618 years after emission onset, simultaneous with the peak in the average surface pH.

Figure 7 shows the  $\delta^{13}\text{C}$  isotope signature for the atmosphere and ocean boxes as a function of time for the case of  $E = 1000 \text{ PgC}$  and  $D = 5 \text{ kyr}$ . The signatures of the surface, intermediate, and deep lines were defined by calculating the unweighted average across basins. The atmosphere and surface ocean perturbations are felt before the deeper ocean boxes. The peak surface signature is 4018 years after emission onset. The peak deep signature occurs 5337 years after emission onset, more than 1300 years after it peaks at the surface.

## 5 Power law scalings

Table 1 compares two cases which differ in  $D$  and  $E$  but share the same  $\Delta R$ . If the system response was linear we would expect the perturbations in these two cases to

104

be in proportion to  $E$ , i.e., differ in their response by 20×. However, Table 1 shows that none of these variables are in the proportion of 20 : 1. Alternatively, if the response were nonlinear but depended only on  $\Delta R$ , we would expect these variables to be in constant proportion other than 20 : 1. This not the case either. Accordingly, a more  
 5 general formulation is needed to systematize these results.

A power law relationship between the the peak change in a system variable  $\Delta V$  and the total magnitude and duration of the emission event shown in Fig. 1 can be written as

$$\Delta V = \gamma D^\alpha E^\beta \quad (5)$$

10 where the coefficient  $\gamma$  and the exponents  $\alpha$  and  $\beta$  assume different values for each system variable. Alternatively, Eq. (5) can be written in terms of emission rate using  $\Delta R = 2E/D$ ,

$$\Delta V = 2^{-\beta} \gamma D^{\alpha+\beta} \Delta R^\beta = 2^\alpha \gamma E^{\alpha+\beta} \Delta R^{-\alpha} \quad (6)$$

If the peak change in  $\Delta V$  depends only on the peak emissions rate,  $\Delta R$ , as suggested for the atmosphere by the simple equilibrium balance between volcanic  
 15 emission and silicate weathering fluxes, then we expect  $\alpha = -\beta$  in Eqs. (5) and (6). Other simple balances are possible. For example, it may be that the peak values depend on the actual time varying emissions rate  $R'(t) = R(t) - R_0$ . In LOSCAR the evolution of atmospheric  $\text{CO}_2$  is determined by

$$20 \frac{d}{dt}(\text{TC}_{\text{atm}}) = F_{\text{vc}} + F_{\text{gas}} - F_{\text{cc}} - 2F_{\text{si}} + R' \quad (7)$$

where  $F_{\text{vc}}$  is the flux due to volcanic degassing,  $F_{\text{gas}}$  is the flux due to air–sea gas exchanges,  $F_{\text{cc}}$  and  $F_{\text{si}}$  are the carbonate and silicate weathering fluxes respectively, and  $R'$  is the flux from emissions. The weathering fluxes  $F_{\text{cc}}$  and  $F_{\text{si}}$  are parameterized in LOSCAR in the following form (Zeebe, 2012b; Walker et al., 1981; Berner et al.,

105

1983; Walker and Kasting, 1992):

$$F_{\text{cc}} = F_{\text{cc}}^0 \left( \frac{\rho\text{CO}_2}{\rho\text{CO}_2^0} \right)^{\text{ncc}} \quad (8)$$

$$F_{\text{si}} = F_{\text{si}}^0 \left( \frac{\rho\text{CO}_2}{\rho\text{CO}_2^0} \right)^{\text{nsi}} \quad (9)$$

Where the superscript 0 refers to the long-term steady state, and ncc and nsi are constant exponents. As described in Zeebe (2012b) the long-term steady state of  
 5  $\rho\text{CO}_2$  in LOSCAR is reached via removal of atmospheric carbon through weathering of silicates and subsequent burial as marine carbonate sediments. Following emissions onset, Eq. (7) reduces approximately to a long-term flux balance in which  $F_{\text{vc}} = F_{\text{si}}$ .

$$F_{\text{si}} \propto R' \quad (10)$$

10 since

$$F_{\text{si}} \propto (\rho\text{CO}_2)^{\text{nsi}} \quad (11)$$

Equation (10) yields

$$\rho\text{CO}_2 \propto (R')^{\frac{1}{\text{nsi}}} \quad (12)$$

15 which suggests that the change in atmospheric carbon should scale with  $R'$  and exhibit a  $1/\text{nsi}$  sensitivity. Because nsi is usually assumed to be relatively small, a very strong sensitivity of climate to emissions is implied by Eq. (12).

Our scaling analysis considers only peak values of the perturbed variables. To determine global ocean carbon content we multiplied the dissolved inorganic carbon (DIC) concentrations in each of the ocean boxes by their prescribed volumes to obtain  
 20 the total mass of carbon in each box. We then summed over all the ocean boxes to



ncc at the default value, also results in negligible changes in the  $\alpha$  values. Figure 11f shows that as ncc increases while holding nsi at the default value, the resulting  $\beta$  values for TA monotonically increase; similar to the behavior in Fig. 11d. Also increasing nsi, while holding ncc at the default value, yields smaller  $\beta$  values like those in Fig. 11d.  
5 In summary Fig. 11 shows that  $\beta$  values are relatively more sensitive to changes in weathering strengths, but that sensitivity is much weaker than would be anticipated from the two term atmospheric balance.

## 7 Discussion

The results presented in the previous section raise a number of important questions. 10 In this section we further examine these, in particular – (1) Why is the dependence on weathering so weak? (2) What controls the maximum in  $\text{CO}_2$ ? And (3) What does this imply about additional feedbacks in the system?

Considerable insight can be gained into how the maximum  $p\text{CO}_2$  is set by noting that the bicarbonate ion concentration at equilibrium is given by

$$15 \quad [\text{HCO}_3^-] = \frac{k_H k_1 p\text{CO}_2}{[\text{H}^+]}. \quad (13)$$

where  $k_H$  is the Henry's law coefficient and  $k_1$  is a dissociation coefficient, and  $[\text{H}^+]$  is the hydrogen ion concentration. Similarly, the equilibrium carbonate ion concentration is given by

$$[\text{CO}_3^{2-}] = \frac{k_H k_1 k_2 p\text{CO}_2}{[\text{H}^+]^2}. \quad (14)$$

20 Then we can solve for the  $p\text{CO}_2$  from Eqs. (13) and (14)

$$p\text{CO}_2 = \frac{k_2 [\text{HCO}_3^-]^2}{k_H k_1 [\text{CO}_3^{2-}]} \quad (15)$$

109

Letting TDIC denote the total dissolved inorganic carbon and TA the total alkalinity, we can approximate Eq. (15) as in Sarmiento and Gruber (2006) by

$$p\text{CO}_2 \approx \frac{k_2}{k_H k_1} \frac{(2\text{TDIC} - \text{TA})^2}{\text{TA} - \text{TDIC}} \quad (16)$$

This approximation is only valid when the aqueous  $\text{CO}_2$  is small in comparison 5 with the carbonate ion concentration, as it is in the modern ocean. However, the additional mathematical complexity that results from adding aqueous  $p\text{CO}_2$  to Eq. (16), (converting it to a quadratic equation in  $p\text{CO}_2$ ), largely adds complexity to the solutions developed below without adding much in the way of physical content.

Within this approximation there are two possible ways for  $\partial p\text{CO}_2/\partial t$  to equal zero 10 in Eq. (16). The first is the equilibrium regime where  $\partial\text{TA}/\partial t = \partial\text{TDIC}/\partial t = 0$ . This is the regime in which we would expect to find a strong dependence on weathering parameters. However, as can be seen from looking at Fig. 12, our transient simulations are characterized by a *dynamic* balance where both TDIC and TA are changing. Setting the time derivative of Eq. (16) to zero and rearranging gives

$$15 \quad \frac{\partial\text{TDIC}}{\partial t} = \left( \frac{\text{TA}}{3\text{TDIC} - 2\text{TA}} \right) \frac{\partial\text{TA}}{\partial t} \quad (17)$$

Given that the TDIC and TA are quite similar in size, this implies that a dynamic equilibrium can be achieved when

$$\frac{\partial\text{TA}/\partial t}{\partial\text{TDIC}/\partial t} = \theta \approx 1 \quad (18)$$

This dynamic balance means that it is the growth of alkalinity within the ocean that 20 brings atmospheric  $p\text{CO}_2$  into balance. Examining  $\theta$  at the time of maximum  $p\text{CO}_2$  (Fig. 12a) shows that the two terms are approximately the same for all the runs with durations of 5000, 25 000 and 100 000 years. This makes sense because the uptake of



carbon in the short-duration cases is determined by the ability of the ocean circulation to move carbon away from the surface rather than by weathering feedbacks. Indeed, careful examination of these cases shows that the bulk of added carbon dioxide resides in the atmosphere. However, as the duration of the emissions pulse becomes long in comparison with the overturning timescale of the oceans, the basic balance in Eq. (18) holds.

The relatively weak dependence of  $\theta$  on total emissions obscures an interesting difference between short and long-duration pulses. For short-duration pulses,  $\theta$  increases as the emissions increase. As more and more carbon is added to the system over short periods of time, more of it reacts with calcium carbonate, and increases ocean alkalinity. However, for the long-duration simulations, the dependence runs in the opposite direction, with higher emissions showing less compensation from alkalinity.

To first-order, a situation in which the growth rates in TDIC and TA are equal is what one would expect in a system without burial, where the additional carbon added to the atmosphere reacts with silicate rocks, and the additional alkalinity ends up accumulating in the ocean. Such a situation would also be expected to have a strong dependence on weathering parameters. However, in LOSCAR the dominant flux of alkalinity is often from the sediments to the ocean. This flux will grow not just because the deep ocean pH increases, but because more sediments are mobilized as this happens. Note that the discretization of the deep ocean into a fixed number of boxes introduces some step-like behavior in the volume of sediments mobilized, which can be seen in Fig. 12b. The fact that less sediment is available for interaction as the lysocline shallows may explain part of why  $\theta$  drops at high emission in Fig. 12b. In any case, we expect the sediment alkalinity flux to have a functional dependence on the perturbation DIC, which is linear or superlinear, implying that it has the potential to overwhelm the rather weak dependence on  $p\text{CO}_2$  prescribed generally used in Eqs. (8) and (9).

The importance of sediment interactions may explain why LOSCAR gives different results than other models. For example, recent work by Cui et al. (2013) examines the carbon-13 isotope anomaly at the end of the Permian using the cGENIE model

of Ridgwell and Hargreaves (2007). In that model an atmospheric perturbation of around 17 500 Pg biogenic carbon with an isotope anomaly of  $-25\text{‰}$  is associated with a carbon-13 anomaly of around  $3\text{‰}$  in shallow carbonates lasting about 60 000 years. Our scaling would predict such an isotopic anomaly in surface waters would be associated with a total emission of only about 8000 PgC. Moreover, because much of this carbon interacts with sediments, only 1143 PgC ends up in the atmosphere at the peak, causing a much smaller perturbation to global climate.

Furthermore, our results suggest other important sensitivity studies. In particular, the strong role played by the oceanic carbonate budget suggests additional feedbacks involving the biological pump. In the version of LOSCAR used here, the removal of organic material from the surface layer is primarily controlled by high-latitude nutrients and the ocean circulation, neither of which varies with  $\text{CO}_2$  in our simulations. Additionally, the rain ratio of particulate inorganic carbon to organic carbon is held constant. All of these are likely to vary in the real world.

However, it should also be noted that a robust connection between these changes in the biological pump and climate remains uncertain. For example, today the deep ocean receives water injected from the North Atlantic, which in the modern world has relatively low surface nutrients, and the Southern Ocean, which has relatively high surface nutrients. As noted by Marinov et al. (2008), changes in the balance of deep waters formed from these regions can significantly alter the carbon stored by the biological pump in the deep ocean, so that a slowdown in circulation may produce either increased or decreased storage of carbon (with corresponding changes in deep ocean acidity). While one might expect the total level of vertical exchange to decrease as atmospheric carbon dioxide increases, it is much less clear how the balance between the two sources regions would change.

Similarly, there are open questions regarding the rain ratio. While it does seem likely that this value will be a function of carbon saturation state, it is not clear what the dependence should be. While some calcifying organisms like corals (Langdon et al., 2000) and pteropods (Fabry et al., 2008) tend to grow more slowly under higher levels



- Sluijs, A., Zeebe, R. E., Bijl, P. K., and Bohaty, S. M.: A middle Eocene carbon cycle conundrum, *Nat. Geosci.*, 6, 429–434, 2013. 99
- Stuecker, M. F. and Zeebe, R. E.: Ocean chemistry and atmospheric CO<sub>2</sub> sensitivity to carbon perturbations throughout the Cenozoic, *Geophys. Res. Lett.*, 37, L03609, doi:10.1029/2009GL041436, 2010. 99
- 5 Tjiputra, J. F., Assmann, K., Bentsen, M., Bethke, I., Otterå, O. H., Sturm, C., and Heinze, C.: Bergen earth system model (BCM-C): model description and regional climate-carbon cycle feedbacks assessment, *Geosci. Model Dev.*, 3, 123–141, doi:10.5194/gmd-3-123-2010, 2010. 98
- 10 Uchikawa, J. and Zeebe, R. E.: Influence of terrestrial weathering on ocean acidification and the next glacial inception, *Geophys. Res. Lett.*, 35, L23608, doi:10.1029/2008GL035963, 2008. 97, 99, 108
- Uchikawa, J. and Zeebe, R. E.: Examining possible effects of seawater pH decline on foraminiferal stable isotopes during the Paleocene-Eocene Thermal Maximum, *Paleoceanography*, 25, PA2216, doi:10.1029/2009PA001864, 2010. 99
- 15 Walker, J. C. G. and Kasting, J. F.: Effects of fuel and forest conservation on future levels of atmospheric carbon dioxide, *Palaeogeography, Palaeoclimatology, Paleoecology, Global Planet. Change*, 97, 151–189, 1992. 106
- Walker, J. C. G., Hays, P. B., and Kasting, J. F.: A negative feedback mechanism for the long-term stabilization of Earth's surface temperature, *J. Geophys. Res.*, 86, 9776–9782, 1981. 20 97, 105
- Zeebe, R. E.: History of seawater carbonate chemistry, atmospheric CO<sub>2</sub>, and ocean acidification, *Annu. Rev. Earth Pl. Sc.*, 40, 141–165, 2012a. 99
- Zeebe, R. E.: LOSCAR: Long-term Ocean-atmosphere-Sediment CARbon cycle Reservoir Model v2.0.4, *Geosci. Model Dev.*, 5, 149–166, doi:10.5194/gmd-5-149-2012, 2012b. 25 97, 98, 100, 103, 105, 106, 108
- Zeebe, R. E. and Zachos, J. C.: Long-term legacy of massive carbon input to the Earth system: Anthropocene vs. Eocene, *Philos. T. R. Soc. Lond.*, 371, 20120006, doi:10.1098/rsta.2012.0006, 2013. 99
- 30 Zeebe, R. E., Zachos, J. C., Caldeira, K., and Tyrrell, T.: Carbon emissions and acidification, *Science*, 321, 51–52, 2008. 99

- Zeebe, R. E., Zachos, J. C., and Dickens, G. R.: Carbon dioxide forcing alone insufficient to explain Palaeocene-Eocene thermal maximum warming, *Nat. Geosci.*, 2, 576–580, 2009. 98, 99

**Table 1.** Comparison of cases.

$\Delta V$	Units	Case 1	Case 2	Case 2 : Case 1
$TC_{atm}$	PgC	158.313	2123.627	13.41
$TC_{ocn}$	PgC	$0.1681 \times 10^4$	$3.0729 \times 10^4$	18.28
TA	mol	$0.1354 \times 10^{18}$	$2.4707 \times 10^{18}$	18.25
$\delta^{13}C_{atm}$	‰	1.009	3.550	3.52
$\delta^{13}C_S$	‰	1.036	4.775	4.61
$\delta^{13}C_M$	‰	0.686	4.955	7.22
$\delta^{13}C_D$	‰	0.873	12.188	13.96

**Table 2.** Summary of weathering strength variations considered.

nsi	0.20*	0.20	0.20	0.20	0.20	0.025	0.10	0.40	2.0
ncc	0.40*	0.025	0.05	0.80	2.0	0.40	0.40	0.40	0.40

\* indicates LOSCAR default values.

**Table 3.** Variable definitions and symbols used.

Variable	Symbol	Units
Atmosphere	atm	NA
Ocean	ocn	NA
Sediments	sed	NA
High Latitude, Atlantic, Indian, Pacific Basins	H, A, I, P	NA
Surface, Intermediate, Deep Ocean Boxes	S, M, D	NA
Emissions Rate	$R$	PgCyr <sup>-1</sup>
Emissions Duration	$D$	yr
Total Emissions	$E$	PgC
System Variable	$V$	Varies
Coefficient	$\gamma$	Varies
Duration Scaling Exponent	$\alpha$	ND
Emissions Scaling Exponent	$\beta$	ND
Global Total Alkalinity	TA	mol
pH	pH	ND
Temperature	$T$	°C
Sediment Carbonate Weight %	% CaCO <sub>3</sub>	ND
Time	$t$	yr
Total Atmospheric Carbon	TC <sub>atm</sub>	PgC
Total Oceanic Carbon	TC <sub>ocn</sub>	PgC
Carbon-13 Isotope	$\delta^{13}\text{C}$	‰
Volcanic Degassing Flux	$F_{\text{vc}}$	PgCyr <sup>-1</sup>
Air–Sea Gas Exchange Flux	$F_{\text{gas}}$	PgCyr <sup>-1</sup>
Carbonate Weathering Flux	$F_{\text{cc}}$	PgCyr <sup>-1</sup>
Silicate Weathering Flux	$F_{\text{si}}$	PgCyr <sup>-1</sup>
Emissions Flux	$R'$	PgCyr <sup>-1</sup>
Silicate Weathering Exponent	nsi	ND
Carbonate Weathering Exponent	ncc	ND
Calcite Compensation Depth	CCD	km
Carbonate Ion	CO <sub>3</sub> <sup>2-</sup>	mol

**Table 4.** Power law scalings, global variables,  $\Delta V = \gamma D^\alpha E^\beta$ .  $D$  in [yr] and  $E$  in [PgC].

$V$	Units	$\gamma$	$\alpha$	$\beta$	$R$ value
TC <sub>atm</sub>	PgC	0.680	-0.32	1.22	0.986
$T_{\text{atm}}$	°C	0.029	-0.20	0.79	0.974
TC <sub>ocn</sub>	PgC	1.941	-0.003	0.98	0.999
TA	mol	$1.56 \times 10^{14}$	-0.003	0.98	0.999
max TCO <sub>3</sub> <sup>2-</sup>	mol	$1.67 \times 10^{12}$	$1.0 \times 10^{-5}$	0.99	0.995
min TCO <sub>3</sub> <sup>2-</sup>	mol	$3.00 \times 10^{14}$	-0.23	0.77	0.855

**Table 5.** Power law scalings,  $\delta^{13}\text{C}$  variables,  $\Delta V = \gamma D^\alpha E^\beta$ .  $D$  in [yr] and  $E$  in [PgC].

$V$	Units	$\gamma$	$\alpha$	$\beta$	$R$ value
min $\delta^{13}\text{C}_{\text{atm}}$	‰	0.087	-0.268	0.70	0.948
min $\delta^{13}\text{C}_{\text{S}}$	‰	0.045	-0.228	0.75	0.969
min $\delta^{13}\text{C}_{\text{M}}$	‰	0.009	-0.137	0.81	0.983
min $\delta^{13}\text{C}_{\text{D}}$	‰	0.002	-0.035	0.87	0.983

**Table 6.** Power law scaling, ocean boxes,  $\Delta V = \gamma D^\alpha E^\beta$ .  $D$  in [yr] and  $E$  in [PgC].

$V$	Units	$\gamma$	$\alpha$	$\beta$	$R$ value
$\text{TA}_{\text{S}}$	PgC	$4.63 \times 10^{-2}$	$-2.65 \times 10^{-3}$	0.98	0.999
$\text{TA}_{\text{M}}$	PgC	$4.13 \times 10^{-1}$	$-2.64 \times 10^{-3}$	0.98	0.999
$\text{TA}_{\text{D}}$	PgC	1.39	$-2.58 \times 10^{-3}$	0.98	0.999
$\text{TA}_{\text{HL}}$	PgC	$1.27 \times 10^{-2}$	$-2.63 \times 10^{-3}$	0.98	0.999
$\text{TDIC}_{\text{S}}$	PgC	$7.7 \times 10^{-2}$	$-1.64 \times 10^{-2}$	0.94	0.999
$\text{TDIC}_{\text{M}}$	PgC	0.42	$-2.75 \times 10^{-3}$	0.98	0.999
$\text{TDIC}_{\text{D}}$	PgC	1.46	$-2.70 \times 10^{-3}$	0.98	0.999
$\text{TDIC}_{\text{HL}}$	PgC	$1.33 \times 10^{-2}$	$-2.79 \times 10^{-3}$	0.98	0.999
$T_{\text{S}}$	°C	$2.93 \times 10^{-2}$	-0.20	0.79	0.974
$T_{\text{M}}$	°C	$1.28 \times 10^{-2}$	-0.16	0.83	0.974
$T_{\text{D}}$	°C	$4.81 \times 10^{-3}$	-0.09	0.87	0.972
min $\text{pH}_{\text{S}}$	ND	$2.52 \times 10^{-3}$	-0.26	0.83	0.969
min $\text{pH}_{\text{M}}$	ND	$2.01 \times 10^{-3}$	-0.23	0.82	0.936
min $\text{pH}_{\text{D}}$	ND	$5.38 \times 10^{-4}$	-0.14	0.86	0.951
min $\text{CO}_2^{\text{atm}}$	mol	$5.25 \times 10^{13}$	-0.37	0.78	0.868
min $\text{CO}_2^{\text{M}}$	mol	$2.30 \times 10^{14}$	-0.28	0.72	0.836
min $\text{CO}_2^{\text{D}}$	mol	$1.45 \times 10^{14}$	-0.20	0.77	0.864
min $\text{CO}_2^{\text{HL}}$	mol	$9.08 \times 10^{12}$	-0.31	0.74	0.883
max $\text{CO}_2^{\text{atm}}$	mol	$2.13 \times 10^{11}$	$2.50 \times 10^{-3}$	0.92	0.996
max $\text{CO}_2^{\text{M}}$	mol	$7.75 \times 10^{11}$	$4.00 \times 10^{-4}$	0.97	0.997
max $\text{CO}_2^{\text{D}}$	mol	$7.75 \times 10^{11}$	$-1.48 \times 10^{-3}$	1.01	0.993
max $\text{CO}_2^{\text{HL}}$	mol	$1.58 \times 10^{10}$	$4.33 \times 10^{-3}$	0.94	0.989
max $\text{CCD}_{\text{A}}$	km	$2.75 \times 10^{-4}$	-0.01	0.82	0.912
max $\text{CCD}_{\text{I}}$	km	$1.89 \times 10^{-5}$	0.01	1.16	0.923
max $\text{CCD}_{\text{P}}$	km	$4.71 \times 10^{-6}$	-0.01	1.32	0.926
min $\text{CCD}_{\text{A}}$	km	$1.10 \times 10^{-2}$	-0.19	0.75	0.878
min $\text{CCD}_{\text{I}}$	km	$6.41 \times 10^{-4}$	-0.26	1.09	0.815
min $\text{CCD}_{\text{P}}$	km	$1.98 \times 10^{-4}$	-0.23	1.19	0.813

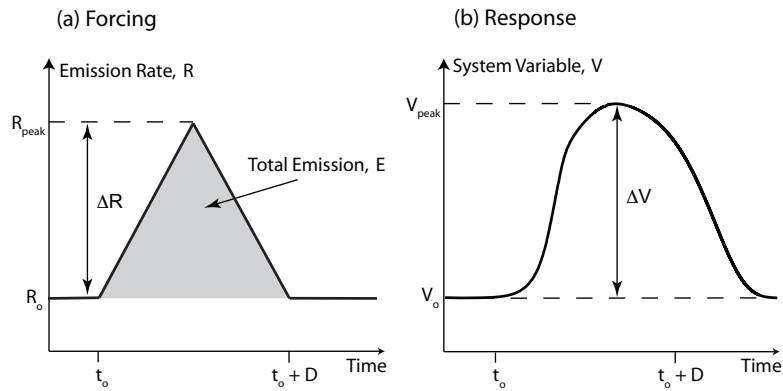


**Figure 1.** Schematic representations of the forcing and nature of system response. **(a)** Triangular atmospheric CO<sub>2</sub> perturbation characterized by duration,  $D$ , and total size of emission,  $E$ . **(b)** Typical system variable response to forcing. We define the peak system response as  $\Delta V = |V_{\text{peak}} - V_0|$ .

123

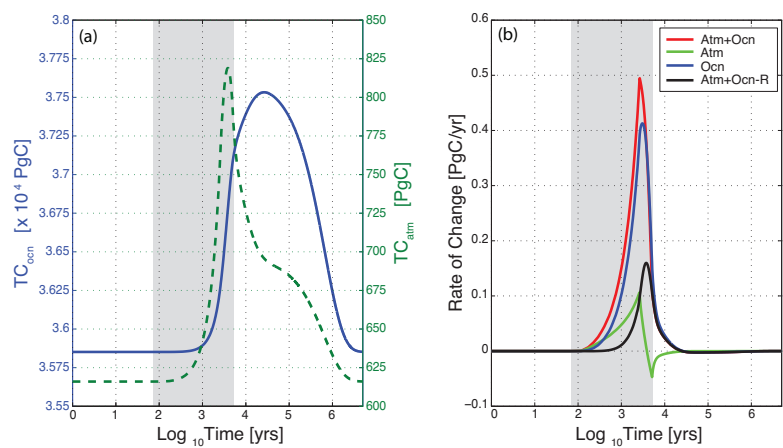


**Figure 2.** System response as a function of time for the case of  $E = 1000$  PgC and  $D = 5$  kyr. Shaded regions indicate time of emission. **(a)** Total carbon in the atmospheric and oceanic reservoirs. **(b)** Corresponding rates of change.

124

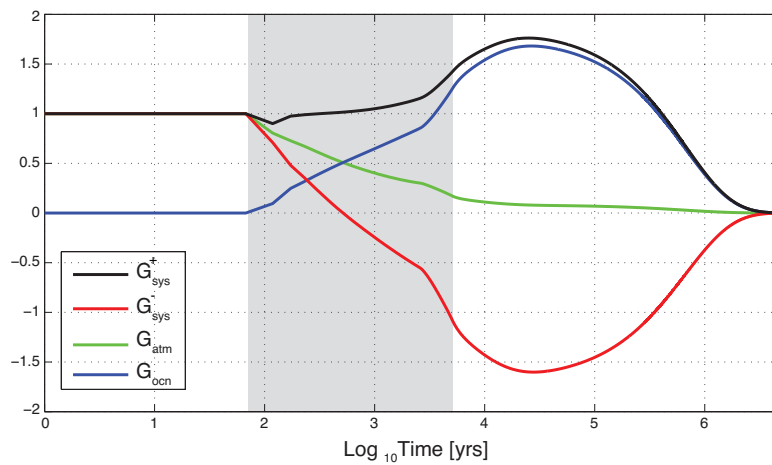


**Figure 3.** System gain factors as a function of time for the case of  $E = 1000$  PgC and  $D = 5$  kyr. Shaded region indicates time of emission.

125

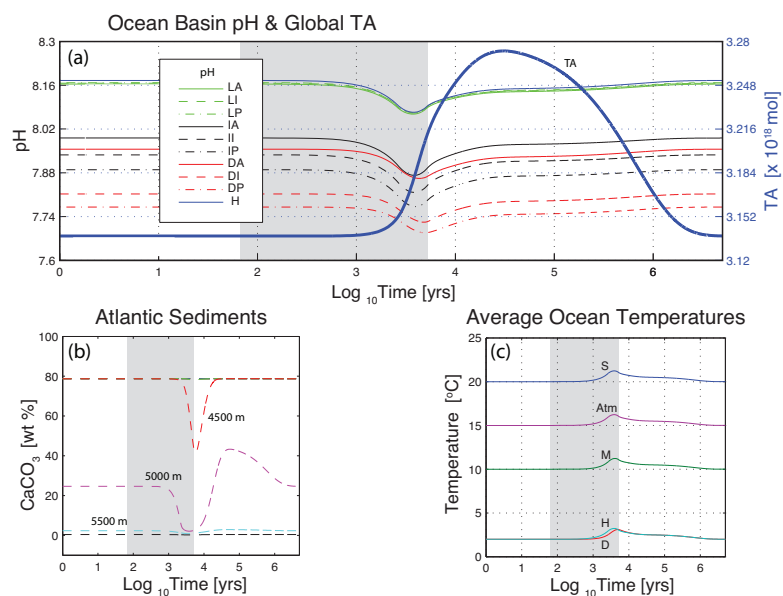


**Figure 4.** System variables as a function of time for the case of  $E = 1000$  PgC and  $D = 5$  kyr. Shaded regions indicate time of emission. (a) Thin lines are pH for ocean boxes. Thick solid line is the global ocean total alkalinity (TA). (b)  $\text{CaCO}_3$  wt% of sediment boxes within the Atlantic basin. (c) Temperature for atmosphere and high-latitude boxes. Surface, intermediate, and deep ocean temperatures are averages across basins.

126



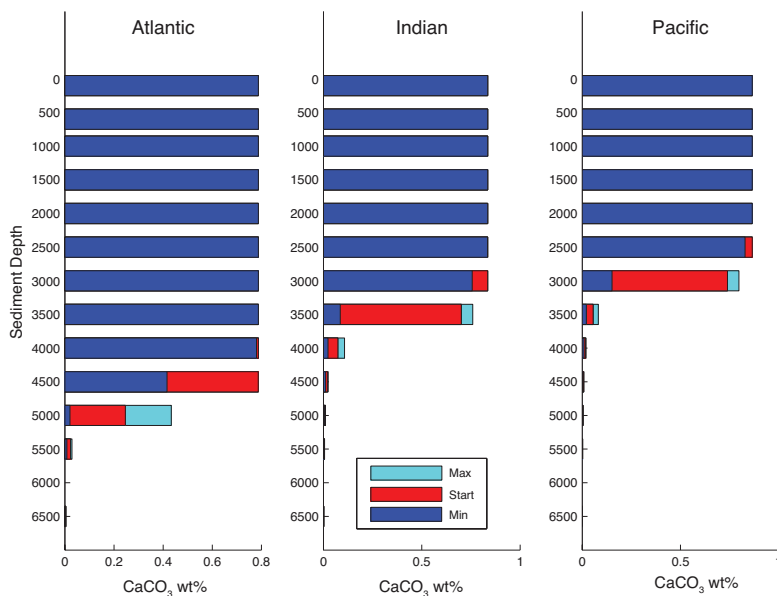


**Figure 5.** Extreme CaCO<sub>3</sub> contents in each ocean basin as a function of sediment depth for the case of  $E = 1000$  PgC and  $D = 5$  kyr.

127

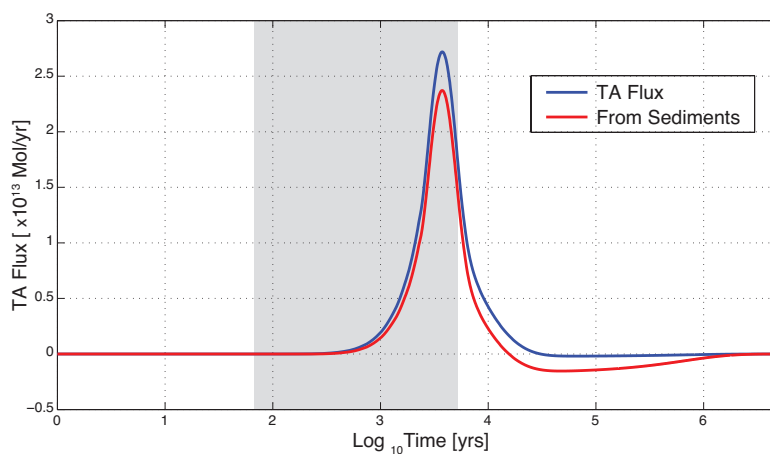


**Figure 6.** Time rate of change of global total alkalinity (TA) for the case of  $E = 1000$  PgC and  $D = 5$  kyr. Shaded region indicates time of emission. Blue curve is the time rate of change of global ocean TA. Red curve shows the blue curve minus the TA flux that is due to weathering feedbacks.

128

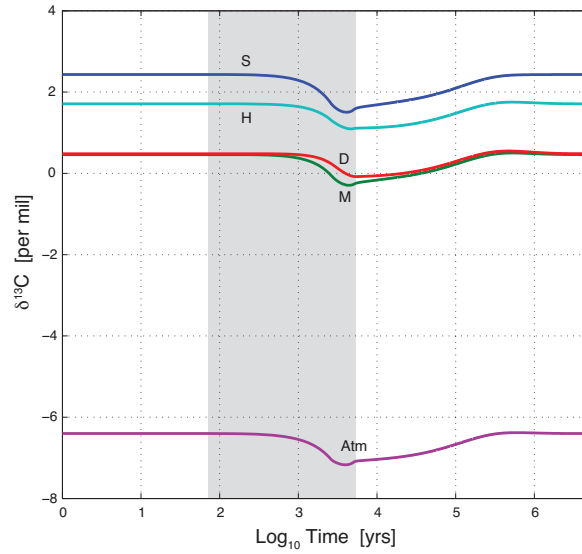


**Figure 7.** Carbon-13 isotope signature for the atmosphere (Atm) and ocean boxes as a function of time for the case of  $E = 1000 \text{ PgC}$  and  $D = 5 \text{ kyr}$ . The surface (S), intermediate (M), and deep (D) boxes were averaged for all basins. H is high latitude box. Shaded region indicates time of emission.

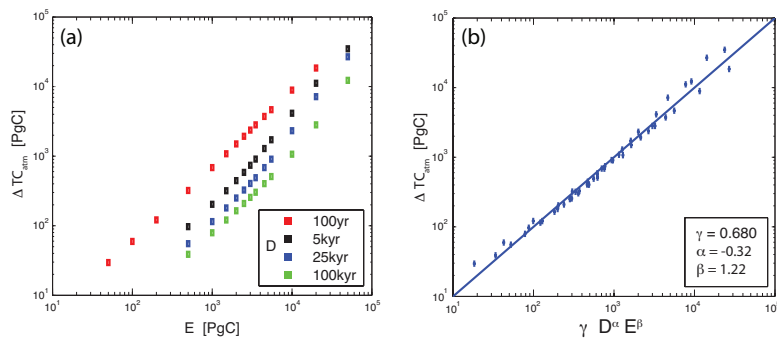


**Figure 8. (a)** Peak changes in the atmospheric total carbon content as a function of total emission,  $E$ , for various durations,  $D$ . **(b)** Multi-variable regression results. Solid line indicates a perfect fit to the predicted scaling. The (+) signs are each individual cases.

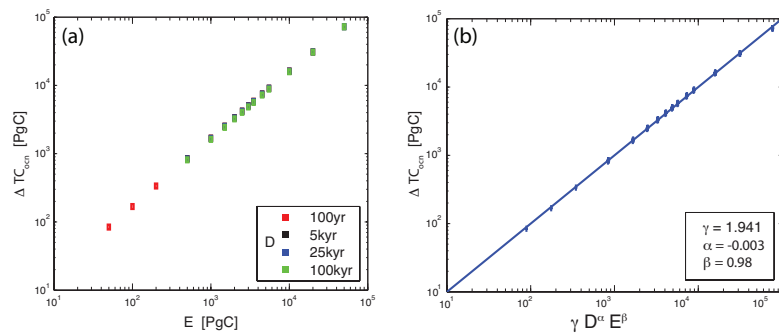


**Figure 9.** (a) Peak changes in the oceanic total carbon content as a function of total emission,  $E$ , for various durations,  $D$ . (b) Multi-variable regression results. Solid line indicates a perfect fit to the predicted scaling. The (+) signs are each individual cases.

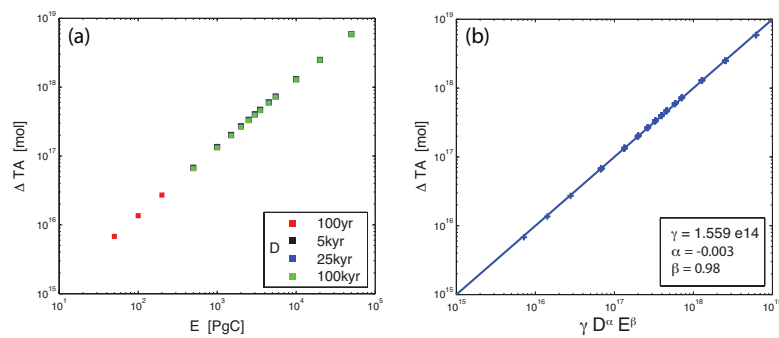


**Figure 10.** (a) Peak changes in the global ocean total alkalinity (TA) as a function of total emission,  $E$ , for various durations,  $D$ . (b) Multi-variable regression results. Solid line indicates a perfect fit to the predicted scaling. The (+) signs are each individual cases.

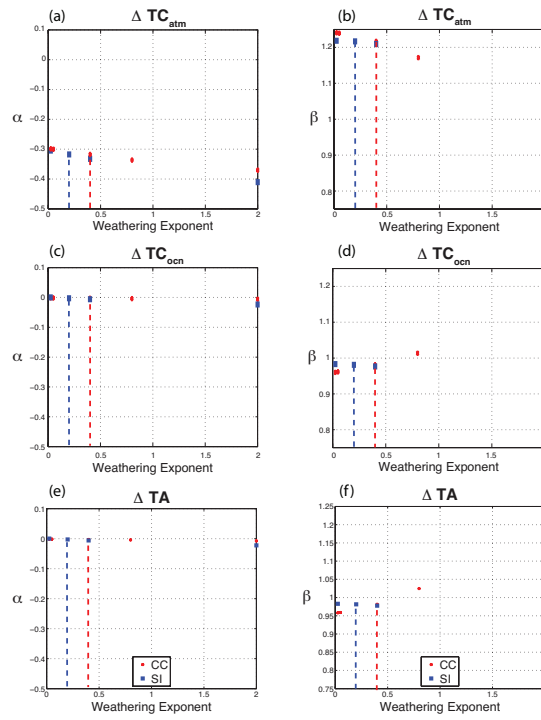


**Figure 11.** Sensitivity of scaling results to variations in weathering exponents. Dashed lines indicate default LOSCAR exponent values ( $n_{cc} = 0.40$ ,  $n_{si} = 0.20$ ). **(a, b)** Peak total atmospheric carbon, **(c, d)** peak total ocean carbon, **(e, f)** peak global total alkalinity (TA).

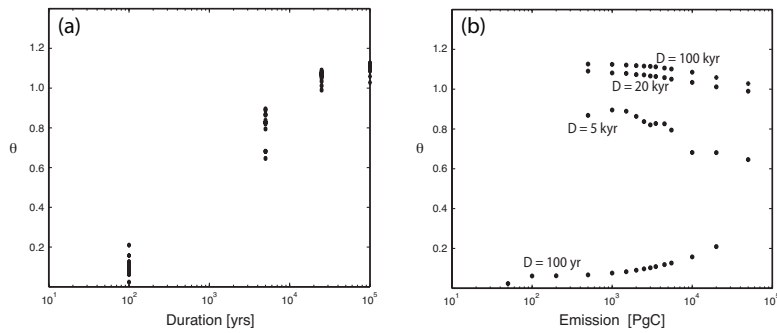


**Figure 12.** Ratio of the rate of change in total global dissolved inorganic carbon to the rate of change in global total alkalinity **(a)** vs. duration, at the time of maximum  $pCO_2$ , and **(b)** vs. emission, at the time of maximum  $pCO_2$ .